

# The sign of kurtosis within finite system near the QCD critical point\*

Shanjin Wu<sup>1,†</sup>

<sup>1</sup>*School of Nuclear Science and Technology, Lanzhou University, Lanzhou 730000, China*

The sign of higher order multiplicity fluctuations is a very important quantity in exploring the QCD phase transition. It is found that the kurtosis of net-baryon is typically negative in the simulations of the dynamics of conserved net-baryon density near the QCD critical point. This paper considers the effects of finite size on the multiplicity fluctuations with equilibrium critical fluctuations. It is found that the multiplicity fluctuations (or magnitude of correlation function  $D_{ij}$ ) are dramatically suppressed with decreasing system size when the size of the system is small comparing correlation length, which is the so-called acceptance dependence. Consequently, the small correlation function of the small system size results in the magnitude of the negative contribution ( $\sim D_{ij}^4$ ) in the four-point correlation function dominates over the one of positive term ( $\sim D_{ij}^5$ ), and this finite size effects induces a dip structure near the QCD critical point.

Keywords: Relativistic heavy-ion collisions, QCD phase transition, Multiplicity fluctuations, Finite-size effects

## I. INTRODUCTION

Exploring the Quantum Chromodynamics (QCD) phase structure is one of the most important topics in high-energy nuclear physics. Simulations by lattice QCD reveal that the transition from the quark-gluon plasma (QGP) phase to the hadron phase is a crossover at vanishing baryon chemical potential ( $\mu \simeq 0$ ) [1–4]. On the other hand, the effective theories based on QCD predict that this transition is a first-order phase transition at finite chemical potential [5–9]. Therefore, it is natural to conjecture the existence of a QCD critical point between the crossover and first-order phase transition [10, 11].

The characteristic feature of the critical point is the long-range correlation and large fluctuations. After being created in relativistic heavy-ion collisions, the QGP fireball scans the QCD phase diagram during the evolving process and may touch the critical region. Such fluctuating effects may imprint the final observable of the heavy-ion experiments. It was conjectured that the non-monotonic behavior as a function of collision energy can be regarded as one of the signatures of the critical point [12, 13, 15]. The first phase Beam Energy Scan (BES-I) program at RHIC has been performed to scan the QCD phase diagram by tuning the collision energy [14]. Preliminary measurement of the net-proton multiplicity fluctuations has shown such non-monotonic behavior with the energy range from 7.7 to 200 GeV [16, 17]. However, the statistics of the BES-I program are insufficient to conclude the observation of the non-monotonic behavior, and it requires much higher statistics in the coming second phase of BES and FIX target measurements.

Theoretically, the QGP fireball created in relativistic heavy-ion collisions is a complex system and several effects may have an impact on the final behavior of the net-proton multiplicity fluctuations. For instance, due to the rapidly expanding effect, the multiplicity fluctuations may deviate from the equilibrium ones. By considering the dynamical effects

induced by the expanding QGP fireball, people found that the magnitude of the fluctuations can be suppressed [18, 19], the sign can be reversed [20], the maximum of the fluctuations can be moved from the critical point [21]. Therefore, remarkable progress has been achieved in developing the dynamical model near the QCD critical point. For example, the dynamics of the conserved variables (charge, net-baryon) have been developed [22–26] and non-monotonic behavior of the fluctuations with respective to the increasing rapidity acceptance window have been observed [22, 25, 26]. Please see *e.g.*, Refs. [27?–32] for recent reviews.

In particular, the signs of the multiplicity fluctuations are important in exploring the phase structure in heavy-ion experiments. Comparing its magnitude the signs can be regarded as more obvious signatures of the phase transition [13, 34]. It was predicted the non-trivial behavior of the signs of higher order cumulants or moments of conserved quantities near the QCD critical point [13, 34]. By developing the dynamical model near the QCD critical point, it was found that the critical slowing down effects may flip the signs of higher order cumulants [20]. Remarkably, the fourth-order cumulants (or kurtosis) of the multiplicity fluctuations in these conserved dynamical models are typically negative [23–26]. This is hard to achieve with only critical slowing down effects. Because the corresponding memory effects preserve the sign of the static kurtosis above the phase transition curve, which is not always negative [20]. Thus, the sign of kurtosis has not been fully understood yet in such a comprehensive and complex simulation of the conserved dynamical models. This work focuses on the study of the impacts from one of the factors in the conserved dynamical simulation, *i.e.*, finite size effects, on the sign of kurtosis. In the realistic experiment detection with a finite range of acceptance, only part of the system has been collected. This corresponds to the finite size of the system and also the kurtosis is obtained within finite volume in the dynamical models. To understand the typically negative kurtosis near the critical point in the dynamical conserved models, this work is dedicated to pointing out that the finite size of the detected system may also modify the sign of kurtosis, by considering the finite volume when calculating the multiplicity fluctuations in a static system.

\* Supported by the National Natural Science Foundation of China (No.12305143) and the China Postdoctoral Science Foundation under Grant (No. 2023M731467)

† Corresponding author, [shanjinwu@lzu.edu.cn](mailto:shanjinwu@lzu.edu.cn)

## II. MULTIPLICITY FLUCTUATIONS WITHIN FINITE SIZE SYSTEM

Near the phase transition, thermal variables (this work focuses on baryon density  $n_B$ ) strongly fluctuate and the corresponding partition function can be written as the Ginzburg-Landau form [23–26]:

$$Z[\mu] = \int Dn_B \exp\left\{-\frac{1}{T} \int d^3x \left[\frac{m^2}{2} n_B^2 + \frac{K}{2} (\nabla n_B)^2 + \frac{\lambda_3}{3} n_B^3 + \frac{\lambda_4}{4} n_B^4 + \mu n_B\right]\right\}, \quad (1)$$

where  $T$  is temperature. The kinetic term with surface tension  $K$  is a measure for the range of the interaction as well as nonlinear interaction terms.  $m = \sqrt{K}/\xi$  is inversely proportional to the correlation length  $\xi$ .  $\lambda_3$  and  $\lambda_4$  are the coupling constants for three- and four-point correlation, respectively. In relativistic heavy-ion experiments, susceptibility of conserved quantity is regarded as the sensitive observable to the QCD phase transition [27, 34–36], because they represent the magnitude of the response of the systems against external force and therefore encodes the correlation between the particles in the system. In particular, people are more interested in the susceptibility of the conserved thermal quantities, such as charge or net-baryon, as they can be obtained unambiguously from the partition function or the grand potential by taking derivatives:

$$\chi_n = \frac{\partial^n P}{\partial \mu^n}, \quad (2)$$

where the pressure has the form

$$P = \frac{T}{V} \ln Z. \quad (3)$$

where  $V$  is the volume of the system.

The second-order baryon number susceptibility is proportional to the two-point correlator:

$$\chi_2 = \frac{V}{T} (\langle n_B^2 \rangle - \langle n_B \rangle^2), \quad (4)$$

where  $\langle \dots \rangle$  denotes the event-by-event averaging. While the average of the correlator over the coordinate space is evaluated with a finite volume

$$\langle n_B^2 \rangle = V^{-2} \int_V d^3x_1 d^3x_2 \langle n_B(x_1) n_B(x_2) \rangle. \quad (5)$$

Namely, the spatial integration is performed within finite volume  $V$ . Note that  $\langle n_B \rangle = 0$  can be obtained from Eq.(1). The

correlation function  $\langle n_B(x_1) n_B(x_2) \rangle$  can be evaluated with

$$\langle n_B(x_1) n_B(x_2) \rangle = \frac{1}{Z} \frac{\partial^2 Z}{\partial \mu^2} = \frac{T}{(2\pi)^3} \int d^3p \frac{e^{i\mathbf{p}(\mathbf{x}_1 - \mathbf{x}_2)}}{K\mathbf{p}^2 + m^2}, \quad (6)$$

This is the Ornstein-Zernicke form of the correlation function. In the dynamics of the conserved baryon density [23–26], the partition function in Eq.(1) is treated as the effective potential in the stochastic diffusion equation. In the linear limit, the dynamical correlation function can be extended as [37]

$$\begin{aligned} \langle n_B(\mathbf{x}_1) n_B(\mathbf{x}_2) \rangle &= \frac{T}{(2\pi)^3} \int d^3p \frac{e^{i\mathbf{p}(\mathbf{x}_1 - \mathbf{x}_2)}}{K\mathbf{p}^2 + m^2} \exp[-Dt\mathbf{p}^2(K\mathbf{p}^2 + m^2)], \end{aligned} \quad (7)$$

where the factor  $\exp[-Dt\mathbf{p}^2(K\mathbf{p}^2 + m^2)]$  is introduced to describe the diffusion of the correlation function as a function of time  $t$ , and  $D$  is the diffusion coefficient. This factor is introduced merely to take into account the dynamical effects in such a static model and it does not change the following analysis. If the dynamical factor  $\exp[-Dt\mathbf{p}^2(K\mathbf{p}^2 + m^2)]$  been neglected, the spatial integration in Eq. (5) is performed in spherical coordinate with radii  $R$ , and it takes the following form:

$$\langle n_B^2 \rangle = \frac{T}{V} \frac{1}{K} [\xi^2(1 - e^{-R/\xi}) - R\xi e^{-R/\xi}]. \quad (8)$$

In the limit of the infinite large volume  $R \gg \xi$ , the second order baryon number susceptibility approaches to correlation length  $\chi_2 \rightarrow \xi^2$ . This means that the susceptibility of the system is only determined by the correlation length  $\xi$ , not the size of the system  $R$ . This reproduces the previous result in Ref. [12]. It can be understood that the number of correlated particles is determined by  $\xi$ . The particles beyond the correlation length  $\xi$  are uncorrelated and do not contribute to the value of susceptibility. On the other hand, in the limit of small size  $R \ll \xi$ , the second order baryon number susceptibility approaches the system size  $\chi_2 \rightarrow R^2/\sqrt{K}$ . In this limit, the susceptibility of the system strongly enhances with the increasing size of the system. This is the so-called acceptance dependence, which has been proposed [38, 39] and observed in experiments [40]. This can be regarded as another indicator of the long-range correlation. When the susceptibility obtained within a scale  $R$  is smaller than the correlation length  $\xi$ , all the particles detected are correlated with each other. The increasing size  $R$  means more particles correlated and contribute to the susceptibility.

Higher order susceptibilities are important observables for the searching QCD critical point because they are more sensitive to the correlation length and their signs are more obvious observables than the magnitudes considering the complex system in relativistic heavy-ion collisions [12, 34]. The fourth-order susceptibility is given by

$$\chi_4 = \frac{\partial^4 P}{\partial \mu^4} = \left(\frac{V}{T}\right)^4 [\langle n_B^4 \rangle - 3\langle n_B^2 \rangle^2], \quad (9)$$

where the four-point correlation function can be calculated from Eq.(1):

$$\begin{aligned}
& \langle n_B(\mathbf{x}_1)n_B(\mathbf{x}_2)n_B(\mathbf{x}_3)n_B(\mathbf{x}_4) \rangle \\
& = -6\lambda_4 T^3 \int d^3z \prod_{i=1}^4 D_{zi} + 12\lambda_3^2 T^3 \int d^3u d^3v D_{u1} D_{u1} D_{v3} D_{v4} D_{uv} + T^2 (D_{12}D_{34} + D_{13}D_{24} + D_{14}D_{23}) \quad (10)
\end{aligned}$$

where the two-point correlator is defined as  $\langle n_B(\mathbf{x}_i)n_B(\mathbf{x}_j) \rangle \equiv TD_{ij}$ . As this work focuses on the susceptibility, the disconnected diagrams  $T^2(D_{12}D_{34} + D_{13}D_{24} + D_{14}D_{23})$  will be canceled due to the subtraction term in Eq. (9). The spatial average of the four-point correlation function Eq. (10) is also evaluated with finite volume. Please see Appendix A for the detailed expression. The integration can not be performed analytically and evaluated numerically instead in this work.

### III. PARAMETERIZATION AND DISCUSSION

To evaluate various orders of cumulants (or susceptibility) near the QCD critical point, it requires the behavior of correlation length  $\xi$ , coupling constants  $\lambda_3$  and  $\lambda_4$ . Lattice QCD suffers sign problem at large chemical potential [11], and the results in the effective theories based on QCD depend on the input parameters. On the other hand, the system near the QCD critical point is believed to belong to the same universality class with three three-dimensional Ising (3D Ising) model [41–43]. Therefore, the equation of state as well as the coupling constants near the QCD critical point can be mapped from the 3D Ising model.

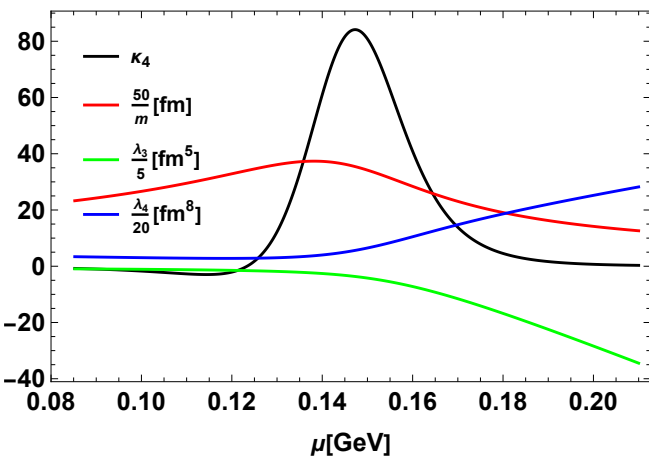


Fig. 1. (Color online) The coupling constants of the effective potential near the critical point, mapped from the 3D Ising model.

To be more specific, in the conserved dynamical model [23–26], the coupling constants are related to the net-

baryon susceptibility in the zero mode limit:

$$\begin{aligned}
\kappa_2 &= \frac{V}{T} \langle n_B^2 \rangle = m^{-2}, \quad \kappa_3 = \left( \frac{V}{T} \right)^2 \langle n_B^3 \rangle = -2\lambda_3 m^{-6}, \\
\kappa_4 &= \left( \frac{V}{T} \right)^3 [\langle n_B^4 \rangle - 3\langle n_B^2 \rangle^2] = 6[2(\lambda_3/m)^2 - \lambda_4] m^{-8}. \quad (11)
\end{aligned}$$

And the net-baryon susceptibilities are mapped from the ones of the 3D Ising model:

$$\kappa_n = T^{4-n} \kappa_n^{\text{Ising}}, \quad (12)$$

where the mapping coefficient is non-universal and  $T^{4-n}$  is chosen according to the dimensional of the baryon susceptibility. In the equation of state for the 3D Ising model, the magnetization  $M$  of the Ising system is a function of the reduced temperature  $r$  and the external magnetic field  $h$  and can be parameterized as [19]:

$$\begin{aligned}
M &= M_0 \tilde{R}^{1/3} \theta, \\
r &= h_0 \tilde{R} (1 - \theta^2), \\
h &= \tilde{R}^{5/3} (3\theta - 2\theta^3). \quad (13)
\end{aligned}$$

with which, various orders of Ising susceptibilities can be obtained by

$$\kappa_{n+1}^{\text{Ising}} = \left. \frac{\partial^n M}{\partial h^n} \right|_r, \quad n = 1, 2, 3, \dots \quad (14)$$

Where  $\tilde{R}$  is the distance to the critical point on the phase diagram, and  $\theta$  is the corresponding angle with respect to the crossover curve.  $M_0$  and  $h_0$  are normalization constants:  $M_0 \simeq 0.605, h_0 \simeq 0.394$ . In addition, the reduced temperature  $r$  and the external magnetic field  $h$  are related to the temperature  $T$  and baryon chemical potential  $\mu$  of QCD system through the linear mapping [20, 21, 26]:

$$\begin{aligned}
\frac{r}{\Delta r} &= -\frac{\mu - \mu_c}{\Delta \mu}, \\
\frac{h}{\Delta h} &= \frac{T - T_c}{\Delta T}. \quad (15)
\end{aligned}$$

where  $T_c$  and  $\mu_c$  are the critical temperature and chemical potential of the QCD critical point, respectively. The critical point of 3D Ising model locates at  $r = h = 0$ . The mapping does not constraint the location of QCD critical point  $(T_c, \mu_c)$ , which are typically treated as free parameters. The behavior of the critical fluctuations are determined by the relative position to the critical point in the QCD phase diagram,

not the absolute value of  $T$  and  $\mu$ . Thus, the location of QCD critical point  $(T_c, \mu_c)$  does not affect the qualitative behavior of  $\kappa\sigma^2$  and are set as  $(T_c, \mu_c) = (0.145 \text{ GeV}, 0.16 \text{ GeV})$  in this work.  $\Delta T$  and  $\Delta\mu$  are the corresponding widths of the critical region,  $\Delta h$  and  $\Delta r$  are the ones in the Ising model. These are non-universal parameters and are set as  $\Delta T = T_c/8, \Delta\mu = 0.1 \text{ GeV}, \Delta r = (5/3)^{3/4}, \Delta h = 1$  in Ref. [26]. Through the mapping, Eq.(14) and Eq. (15), the net-baryon susceptibilities on the QCD phase diagram  $(T, \mu)$  are constructed from the ones on the  $(r, h)$  plane. And therefore the coupling constants can be obtained in Eq. (11).

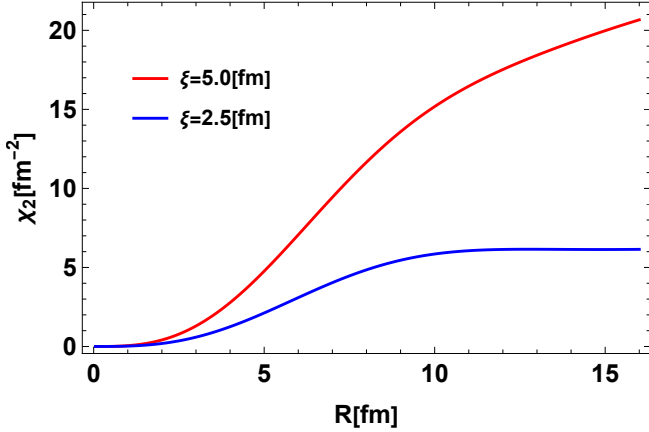


Fig. 2. (Color online) Second order baryon susceptibility  $\chi_2$  as a function of the radius of the coordinate space  $R$ . Different colors represent the input correlation length  $\xi = 2.5 \text{ fm}$  and  $5 \text{ fm}$ .

This work is dedicated to understanding the sign of the kurtosis in the dynamics of the conserved net-baryon near the QCD critical point and the coupling constants are constructed by mapping from the 3D Ising model as in Refs. [23–26]. Fig.1 shows the coupling constants with the temperature  $T = 0.138 \text{ GeV}$ , below the phase transition curve. The fourth-order net-baryon susceptibility constructed from the Ising model has a small negative value at the crossover side (small  $\mu$ ), and becomes positive at the first-order side (large  $\mu$ ). As expected, the coupling constant  $\sqrt{K}/m \equiv \xi$  has a peak close to the critical chemical potential  $\mu_c = 0.16 \text{ GeV}$ . As the constants plotted with the temperature  $T < T_c$ ,  $\lambda_3$  and  $\lambda_4$  have negative and positive values, respectively.

The second-order (4) and fourth-order (9) susceptibilities within the finite system are evaluated with the Monte-Carlo integration algorithm. Since the knowledge of the diffusion constant  $D$  and surface tension  $K$  near the QCD critical point is limited, they are set as  $D = 1 \text{ fm}^{-1}$  and  $K = 1 \text{ fm}^4$ , the evolution time  $t$  is chosen as  $t = 10 \text{ fm}$ . These are treated as free parameters in this work. As shown in Eq. (7), the dynamical factor  $\exp[-Dtp_i^2(Kp_i^2 + m^2)]$  is introduced merely to mimic the dynamical effects in the linearized limit [37]. It is far from realistic dynamical critical fluctuations, which requires full simulation of the dynamical evolution equation [23–26]. The effect of this dynamical factor in this context is suppression of the magnitude of correlation function  $D_{ij}$ . As will be shown below, the sign of  $\kappa\sigma^2$  is determined

by the magnitude of  $D_{ij}$  in this model. Different values of  $D$  and/or  $t$  in this model only impact the critical value of system size  $R$  to get the dip behavior of kurtosis. Fig.2 shows the second-order susceptibility within a finite system as a function of the radius of the system, with different correlation lengths  $\xi$ . One can see that  $\chi_2$  increases monotonically with the increasing size  $R$ . In the case of large correlation length  $\xi = 5.0 \text{ fm}$ ,  $\chi_2$  strongly depends on the size, especially  $R \ll \xi$ , indicating the acceptance dependence of the critical fluctuations in experiments. On the other hand, if the system is much larger than the correlation length (e.g.,  $\xi = 2.5 \text{ fm}$ ),  $\chi_2$  approaches to a constant value when the size is sufficiently large.

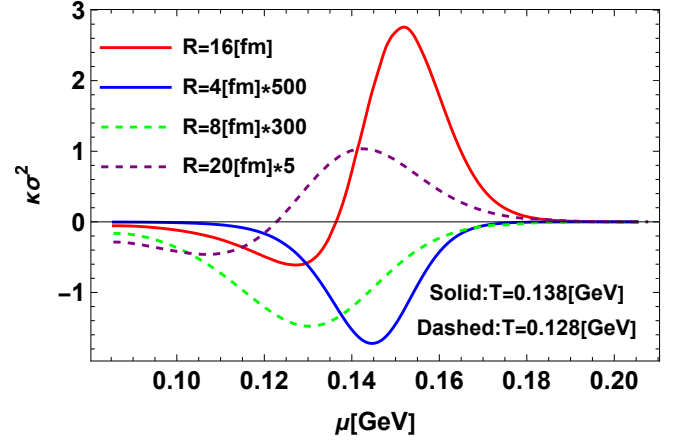


Fig. 3. (Color online) Kurtosis of the net-baryon  $\kappa\sigma^2$  within finite system near the QCD critical point. Different colors correspond to the ones with the radius of the coordinate space  $R = 4, 8, 16, 20 \text{ fm}$ , respectively. Solid curves are obtained with a temperature  $(T = 0.138 \text{ GeV})$  closer to critical temperature  $T_c$ , and the dashed with temperature  $(T = 0.128 \text{ GeV})$  further away from  $T_c$ . The factor after unit means the kurtosis has been multiplied for illustrative purposes (e.g., blue curve corresponds to  $500\kappa\sigma^2$ ).

Fig.3 presents the kurtosis  $\kappa\sigma^2$  of the net-baryon within a finite system near the QCD critical point<sup>3</sup>. In the limit of large system (e.g.,  $R = 16 \text{ fm}$  in Fig.3),  $\kappa\sigma^2$  behaves non-monotonically as a function of the baryon chemical potential  $\mu$  and presents a negative value at crossover side (small  $\mu$ ) and a positive value at first-order side (large  $\mu$ ). This is consistent with the one in an ideal system with infinite large system [13], which can be seen in Eq.(8) that the second order susceptibility approaches to the ideal case  $\chi_2 \rightarrow \xi^2$ . On the other hand,  $\kappa\sigma^2$  within a finite system (e.g.,  $R = 4 \text{ fm}$  in Fig.3) becomes negative and presents a dip behavior near the critical point. As pointed out in Fig.2, the correlation  $D_{ij}$  or the susceptibility strongly depends on the size of the system and has a small value when the system is small. As shown in Eq.(10), the fourth-order coupling term with  $\lambda_4$  presents a negative

<sup>3</sup> Note that Fig.3 only shows the kurtosis with temperature below  $T_c$ , since the kurtosis above  $T_c$  behave similarly as the ones below  $T_c$  because of the symmetry of kurtosis in terms of phase transition curve.



contribution with four terms of correlators  $D_{ij}$ , and the third-order coupling term with  $\lambda_3$  contributes positively with five correlators  $D_{ij}$ s. In the case of a small magnitude of correlator  $D_{ij}$ , the fourth-order coupling term with  $\lambda_4$  dominates and the four-point correlation functions  $\langle n_B^4 \rangle$  can be negative, which results in the negative  $\kappa\sigma^2$  near the QCD critical point. In addition, Fig. 3 also shows the system further away from the critical point ( $T_c = 0.145$  GeV) with temperature  $T = 0.128$  GeV. Comparing the case with  $T = 0.138$  GeV, the critical signal is weaker and the magnitude of  $D_{ij}$  is smaller. The magnitude of  $\kappa\sigma^2$  is smaller (purple curve) and it is easier to achieve the negative kurtosis ( $R = 8$  fm). This means that it is still possible to flip the sign of kurtosis by tuning the system size  $R$  even with different strengths of the critical signal.

Note that  $\kappa\sigma^2$  with  $R = 4$  fm in Fig. 3 has been multiplied by a factor of 500 for illustrative purposes, which is a relatively small value compared with the case of  $R = 16$  fm. It is notable that the model employed in this work is an ideal system, and the quantitative magnitude of the ‘dip’ in the small system size requires more realistic modeling in heavy-ion collisions. QGP fireball created in relativistic heavy-ion collisions is a fast expanding and finite size system, and several factors contribute to the final observables of the QCD critical point. It is typically believed that the dynamical effects ( $\sim \xi^z$ , where the dynamical critical exponent  $z \sim 3$  for QCD critical point) induced by the expanding effects dominate over the finite size effects (finite size of fireball). This motivates the study of the dynamical modeling near the QCD critical point in relativistic heavy-ion collisions [27–32]. However, only part of the system contributes to the final observables considering the finite acceptance window of the detector in experiments. The net-proton multiplicity fluctuations at the Beam Energy Scan phase I already shown the acceptance dependence and the fluctuations with a small acceptance window deviate from the ones with a larger acceptance window [40]. Therefore, the comprehensive dynamical modeling of the critical fluctuations with the realistic detector acceptance window as well as the finite size of the QGP fireball is essential for the comparison with the experiment measurement in the coming Beam Energy Scan phase II.

#### IV. CONCLUSION AND OUTLOOK

In summary, the sign of the higher-order multiplicity fluctuations plays an important role in exploring the QCD phase

transition. In the simulation of the dynamics for the conserved net-baryon density near the QCD critical point, it was found that the kurtosis of net-baryon is typically negative [23–26]. To understand the negative kurtosis in conserved dynamical models, this work focuses on the sign of kurtosis obtained within a finite system, which corresponds to only part of the system being detected. It was found that the susceptibility is proportional to the increasing size of the detected system, and the magnitude of the second-order correlation function  $D_{ij}$  is small when the scale of the system is much smaller than the correlation length. This property, so-called acceptance dependence, results in the negative contribution from the fourth-order coupling term  $\lambda_4$  (proportional to  $\sim D_{ij}^4$ ) dominates in fourth-order susceptibility  $\chi_4$  when the detected system size is small. On the other hand, another term with  $\lambda_3$  (proportional to  $\sim D_{ij}^5$ ) in  $\chi_4$  has a positive contribution that is much smaller than the term with  $\lambda_4$ . In the dynamical models of conserved net-baryon, the kurtosis is obtained only with part of the system, this finite number of particles be detected and the corresponding kurtosis can behave with a dip near the critical point, instead of a peak.

This work focuses on the finite size effects on the sign of kurtosis within the static system without considering the dynamical modeling in a realistic experiment context. Based on the dynamical model near the QCD critical point (e.g., based on hydrodynamic model [23–26] or transport model [44–48]), the realistic finite size of the QGP fireball as well as the finite detector acceptance window requires to be properly taken into account in the future study of higher order net-proton multiplicity fluctuations. In addition, such analysis can also performed with other possible observable of critical point, such light-nuclei yield ratio [49–51].

#### Appendix A: Expression of spatial average of four-point correlation function (10)

This appendix shows the spatial average of the four-point correlation function (10):

$$\langle n_B^4 \rangle = V^{-4} \int_V \prod_{i=1}^4 d^3x_i \langle n_B(x_1) n_B(x_2) n_B(x_3) n_B(x_4) \rangle. \quad (\text{A1})$$

where the detailed expression of the first term is

$$\begin{aligned} & -6\lambda_4 \frac{T^3}{V^4} \int d^3z \int \prod_{i=1}^4 d^3x_i D_{zi} \\ & = -6 \left( \frac{4}{\pi} \right)^3 \frac{\lambda_4 T^3}{V^4} \frac{1}{K^4} \int_0^R dz z^{-2} \int \prod_{i=1}^4 \left[ dp_i \sin(p_i z) (\sin(p_i R) - p_i R \cos(p_i R)) \frac{\exp[-Dtp_i^2(Kp_i^2 + m^2)]}{p_i^2(p_i^2 + m^2/K)} \right], \end{aligned}$$

and the second term is

$$\begin{aligned}
& 12\lambda_3^2 \frac{T^3}{V^4} \int d^3u d^3v \int [d^3x_i] D_{u1} D_{u1} D_{v3} D_{v4} D_{uv} \\
& = 6 \left( \frac{4}{\pi} \right)^4 \frac{\lambda_3^2 T^3}{V^4} \frac{1}{K^5} \int dp_5 \frac{\exp[-Dt p_i^2 (K p_i^2 + m^2)]}{p_5^2 + m^2/K} \int \prod_{i=1}^4 \left[ dp_i (\sin(p_i R) - p_i R \cos(p_i R)) \frac{\exp[-Dt p_i^2 (K p_i^2 + m^2)]}{p_i^2 (p_i^2 + m^2/K)} \right] \\
& \quad \times \int_0^R \frac{dudv}{uv} \sin(p_1 u) \sin(p_2 u) \sin(p_3 v) \sin(p_4 v) \sin(p_5 u) \sin(p_5 v).
\end{aligned}$$

The above integrations can not be performed analytically and are evaluated numerically with the Monte Carlo algorithm.

- 
- [1] Y. Aoki, G. Endrodi, Z. Fodor, et al., The Order of the quantum chromodynamics transition predicted by the standard model of particle physics, *Nature* **443**, 675-678 (2006) doi:10.1038/nature05120
- [2] H. T. Ding, F. Karsch and S. Mukherjee, Thermodynamics of strong-interaction matter from Lattice QCD, *Int. J. Mod. Phys. E* **24**, 1530007 (2015) doi:10.1142/S0218301315300076
- [3] A. Bazavov et al., [USQCD], Hot-dense Lattice QCD: USQCD whitepaper 2018, *Eur. Phys. J. A* **55**, 194 (2019) doi:10.1140/epja/i2019-12922-0
- [4] C. Ratti, Lattice QCD and heavy ion collisions: a review of recent progress, *Rept. Prog. Phys.* **81**, 084301 (2018) doi:10.1088/1361-6633/aabb97
- [5] C. S. Fischer, QCD at finite temperature and chemical potential from Dyson–Schwinger equations, *Prog. Part. Nucl. Phys.* **105**, 1-60 (2019) doi:10.1016/j.ppnp.2019.01.002
- [6] K. Fukushima and T. Hatsuda, The phase diagram of dense QCD, *Rept. Prog. Phys.* **74**, 014001 (2011) doi:10.1088/0034-4885/74/1/014001
- [7] K. Fukushima and C. Sasaki, The phase diagram of nuclear and quark matter at high baryon density, *Prog. Part. Nucl. Phys.* **72**, 99-154 (2013) doi:10.1016/j.ppnp.2013.05.003
- [8] W. j. Fu, QCD at finite temperature and density within the fRG approach: an overview, *Commun. Theor. Phys.* **74**, 097304 (2022) doi:10.1088/1572-9494/ac86be
- [9] W. j. Fu, J. M. Pawłowski and F. Rennecke, QCD phase structure at finite temperature and density, *Phys. Rev. D* **101**, 054032 (2020) doi:10.1103/PhysRevD.101.054032
- [10] M. A. Stephanov, K. Rajagopal and E. V. Shuryak, Signatures of the tricritical point in QCD, *Phys. Rev. Lett.* **81**, 4816-4819 (1998) doi:10.1103/PhysRevLett.81.4816
- [11] M. A. Stephanov, QCD Phase Diagram and the Critical Point, *Prog. Theor. Phys. Suppl.* **153**, 139-156 (2004) doi:10.1143/PTPS.153.139
- [12] M. A. Stephanov, Non-Gaussian fluctuations near the QCD critical point, *Phys. Rev. Lett.* **102**, 032301 (2009) doi:10.1103/PhysRevLett.102.032301
- [13] M. A. Stephanov, On the sign of kurtosis near the QCD critical point, *Phys. Rev. Lett.* **107**, 052301 (2011) doi:10.1103/PhysRevLett.107.052301
- [14] X. Luo and N. Xu, Search for the QCD Critical Point with Fluctuations of Conserved Quantities in Relativistic Heavy-Ion Collisions at RHIC : An Overview, *Nucl. Sci. Tech.* **28**, 112 (2017) doi:10.1007/s41365-017-0257-0
- [15] C. Athanasiou, K. Rajagopal and M. Stephanov, Using Higher Moments of Fluctuations and their Ratios in the Search for the QCD Critical Point, *Phys. Rev. D* **82**, 074008 (2010) doi:10.1103/PhysRevD.82.074008
- [16] J. Adam et al., [STAR], Nonmonotonic Energy Dependence of Net-Proton Number Fluctuations, *Phys. Rev. Lett.* **126**, 092301 (2021) doi:10.1103/PhysRevLett.126.092301
- [17] M. Abdallah et al., [STAR], Cumulants and correlation functions of net-proton, proton, and antiproton multiplicity distributions in Au+Au collisions at energies available at the BNL Relativistic Heavy Ion Collider, *Phys. Rev. C* **104**, 024902 (2021) doi:10.1103/PhysRevC.104.024902
- [18] B. Berdnikov and K. Rajagopal, Slowing out-of-equilibrium near the QCD critical point, *Phys. Rev. D* **61**, 105017 (2000) doi:10.1103/PhysRevD.61.105017
- [19] C. Nonaka and M. Asakawa, Hydrodynamical evolution near the QCD critical end point, *Phys. Rev. C* **71**, 044904 (2005) doi:10.1103/PhysRevC.71.044904
- [20] S. Mukherjee, R. Venugopalan and Y. Yin, Real time evolution of non-Gaussian cumulants in the QCD critical regime, *Phys. Rev. C* **92**, 034912 (2015) doi:10.1103/PhysRevC.92.034912
- [21] S. Tang, S. Wu and H. Song, Dynamical critical fluctuations near the QCD critical point with hydrodynamic cooling rate, *Phys. Rev. C* **108**, 034901 (2023) doi:10.1103/PhysRevC.108.034901
- [22] M. Sakaida, M. Asakawa, H. Fujii et al., Dynamical evolution of critical fluctuations and its observation in heavy ion collisions, *Phys. Rev. C* **95**, 064905 (2017) doi:10.1103/PhysRevC.95.064905
- [23] M. Nahrgang, M. Bluhm, T. Schaefer et al., Diffusive dynamics of critical fluctuations near the QCD critical point, *Phys. Rev. D* **99**, 116015 (2019) doi:10.1103/PhysRevD.99.116015
- [24] M. Nahrgang and M. Bluhm, Modeling the diffusive dynamics of critical fluctuations near the QCD critical point, *Phys. Rev. D* **102**, 094017 (2020) doi:10.1103/PhysRevD.102.094017
- [25] G. Pihan, M. Bluhm, M. Kitazawa et al., Critical net-baryon fluctuations in an expanding system, *Phys. Rev. C* **107**, 014908 (2023) doi:10.1103/PhysRevC.107.014908
- [26] S. Wu, Dynamics of the conserved net-baryon density near QCD critical point within QGP profile, [arXiv:2406.12325 [nucl-th]].
- [27] M. Asakawa and M. Kitazawa, Fluctuations of conserved charges in relativistic heavy ion collisions: An introduction, *Prog. Part. Nucl. Phys.* **90**, 299-342 (2016) doi:10.1016/j.ppnp.2016.04.002
- [28] A. Bzdak, S. Esumi, V. Koch, et al., Mapping the Phases of Quantum Chromodynamics with Beam Energy Scan, *Phys. Rept.* **853**, 1-87 (2020) doi:10.1016/j.physrep.2020.01.005
- [29] M. Bluhm, A. Kalweit, M. Nahrgang, et al., Dynamics of critical fluctuations: Theory – phenomenology –

- heavy-ion collisions, Nucl. Phys. A **1003**, 122016 (2020) doi:10.1016/j.nuclphysa.2020.122016
- [30] S. Wu, C. Shen and H. Song, Dynamically Exploring the QCD Matter at Finite Temperatures and Densities: A Short Review, Chin. Phys. Lett. **38**, 081201 (2021) doi:10.1088/0256-307X/38/8/081201
- [31] X. An, M. Bluhm, L. Du, et al., The BEST framework for the search for the QCD critical point and the chiral magnetic effect, Nucl. Phys. A **1017**, 122343 (2022) doi:10.1016/j.nuclphysa.2021.122343
- [32] L. Du, A. Sorensen and M. Stephanov, The QCD phase diagram and Beam Energy Scan physics: a theory overview, doi:10.1142/S021830132430008X
- [33] J. Chen, J. H. Chen, X. Dong et al., Properties of the QCD matter: review of selected results from the relativistic heavy ion collider beam energy scan (RHIC BES) program, Nucl. Sci. Tech. **35**, 214 (2024) doi:10.1007/s41365-024-01591-2
- [34] M. Asakawa, S. Ejiri and M. Kitazawa, Third moments of conserved charges as probes of QCD phase structure, Phys. Rev. Lett. **103**, 262301 (2009) doi:10.1103/PhysRevLett.103.262301
- [35] M. Kitazawa and M. Asakawa, Revealing baryon number fluctuations from proton number fluctuations in relativistic heavy ion collisions, Phys. Rev. C **85**, 021901 (2012) doi:10.1103/PhysRevC.85.021901
- [36] M. Kitazawa and M. Asakawa, Relation between baryon number fluctuations and experimentally observed proton number fluctuations in relativistic heavy ion collisions, Phys. Rev. C **86**, 024904 (2012) [erratum: Phys. Rev. C **86**, 069902 (2012)] doi:10.1103/PhysRevC.86.024904
- [37] U.C. Tauber, in *Critical Dynamics, A Field Theory Approach to Equilibrium and Non-Equilibrium Scaling Behavior*, Cambridge University Press, New York, 2014
- [38] B. Ling and M. A. Stephanov, Acceptance dependence of fluctuation measures near the QCD critical point, Phys. Rev. C **93**, 034915 (2016) doi:10.1103/PhysRevC.93.034915
- [39] L. Jiang, P. Li and H. Song, Correlated fluctuations near the QCD critical point, Phys. Rev. C **94**, 024918 (2016) doi:10.1103/PhysRevC.94.024918
- [40] X. Luo [STAR], Energy Dependence of Moments of Net-Proton and Net-Charge Multiplicity Distributions at STAR, PoS **CPOD2014**, 019 (2015) doi:10.22323/1.217.0019
- [41] R. D. Pisarski and F. Wilczek, Remarks on the Chiral Phase Transition in Chromodynamics, Phys. Rev. D **29**, 338-341 (1984) doi:10.1103/PhysRevD.29.338
- [42] F. Wilczek, Application of the renormalization group to a second order QCD phase transition, Int. J. Mod. Phys. A **7**, 3911-3925 (1992) [erratum: Int. J. Mod. Phys. A **7**, 6951 (1992)] doi:10.1142/S0217751X92001757
- [43] K. Rajagopal and F. Wilczek, Static and dynamic critical phenomena at a second order QCD phase transition, Nucl. Phys. B **399**, 395-425 (1993) doi:10.1016/0550-3213(93)90502-G
- [44] Q. Chen and G. L. Ma, Phys. Rev. C **106**, no.1, 014907 (2022) doi:10.1103/PhysRevC.106.014907 [arXiv:2207.11736 [nucl-th]].
- [45] Y. Zhou, S. S. Shi, K. Xiao et al., Higher Moments of Net-Baryon Distribution as Probes of QCD Critical Point, Phys. Rev. C **82**, 014905 (2010) doi:10.1103/PhysRevC.82.014905
- [46] J. Xu, S. Yu, F. Liu et al., Cumulants of net-proton, net-kaon, and net-charge multiplicity distributions in Au + Au collisions at  $\sqrt{s_{NN}}=7.7, 11.5, 19.6, 27, 39, 62.4$ , and 200 GeV within the UrQMD model, Phys. Rev. C **94**, 024901 (2016) doi:10.1103/PhysRevC.94.024901
- [47] X. Jin, J. Chen, Z. Lin et al., Explore the QCD phase transition phenomena from a multiphase transport model, Sci. China Phys. Mech. Astron. **62**, 11012 (2019) doi:10.1007/s11433-018-9272-4
- [48] Q. Chen, R. Wen, S. Yin, et al., The influence of hadronic rescatterings on the net-baryon number fluctuations, [arXiv:2402.12823 [nucl-th]].
- [49] C.M. Ko, Searching for QCD critical point with light nuclei. Nucl. Sci. Technol. **34**, 80 (2023). doi.org/ 10. 1007/ s41365-023-01231-1
- [50] K. J. Sun, L. W. Chen, C. M. Ko et al., Light nuclei production as a probe of the QCD phase diagram, Phys. Lett. B **781**, 499-504 (2018) doi:10.1016/j.physletb.2018.04.035
- [51] K. J. Sun, L. W. Chen, C. M. Ko et al., Probing QCD critical fluctuations from light nuclei production in relativistic heavy-ion collisions, Phys. Lett. B **774**, 103-107 (2017) doi:10.1016/j.physletb.2017.09.056